01 Sep 2019

Discontinuous Galerkin vs. IE Method for Electromagnetic Scattering from Composite Metallic and Dielectric Structures

Y.-Y. Zhu

Q.-M. Cai

R. Zhang

X. Cao

et. al. For a complete list of authors, see https://scholarsmine.mst.edu/ele_comeng_facwork/4173

Recommended Citation

Y. Zhu et al., "Discontinuous Galerkin vs. IE Method for Electromagnetic Scattering from Composite Metallic and Dielectric Structures," *Progress In Electromagnetics Research M*, vol. 84, pp. 197-209, Electromagnetics Academy, Sep 2019.
The definitive version is available at https://doi.org/10.2528/PIERM19060701

Progress In Electromagnetics Research M, Vol. 84, 197–209, 2019

Discontinuous Galerkin VSIE Method for Electromagnetic Scattering from Composite Metallic and Dielectric Structures

Yu-Yu Zhu[1], Qiang-Ming Cai[2, *], Runren Zhang[3], Xin Cao[2], Yan-Wen Zhao[1], Bin Gao[1], and Jun Fan[4]

Abstract—In this paper, an efficient volume surface integral equation (VSIE) method with nonconformal discretization is developed for the analysis of electromagnetic scattering from composite metallic and dielectric (CMD) structures. This VSIE scheme utilizes curved tetrahedral (triangular) elements for volume (surface) modeling and the associated CRWG (CSWG) basis functions for volume current (surface) current modeling. Further, a discontinuous Galerkin (DG) volume integral equation (VIE) method and a DG surface integral equation (SIE) approach are adopted for dielectric and metallic parts, respectively, which allow both conformal and nonconformal volume/surface discretization improving meshing flexibility considerably. Numerical results are provided to demonstrate the accuracy, efficiency, and flexibility of our scheme.

1. INTRODUCTION

Numerical modeling of electromagnetic (EM) scattering from composite metallic and dielectric (CMD) structures has applications in many areas, e.g., conformal antennas and radar cross section prediction [1]. One of the competitive methods to model CMD structures is volume surface integral equation (VSIE), a derivative of the method of moments (MoM). In particular, the VSIE approach is more preferred for the objects containing highly inhomogeneous dielectric medias and multiple thin dielectrics with corners and edges, because of the efficiency and accuracy [2].

In earlier studies, VSIE is commonly discretized by RWG [3] and SWG [4] basis functions defined on conformal planar elements. Two problems, however, restrict the VSIE application. On the one hand, large-scale objects will generate a lot of unknowns and therefore lead into high memory and computational time. On the other hand, the planar elements will lose curvature information and introduce additional geometrical modeling error. Moreover, as divergence-conformal bases, RWG and SWG require to be defined on a pair of conformal and adjacent elements and demand high-quality conformal mesh grids to guarantee accuracy. This conformal meshing, however, is nontrivial and sometimes impossible, especially for the CMD objects containing multiscale, high-definition, or inhomogeneous dielectric materials [5].

To alleviate the above problems, integral equation methods, e.g., SIE [6–9], VIE [10–16, 19], VSIE [17, 18], with nonconformal discretization have been extensively studied. In [6] and [7], by introducing half RWG basis functions, the SIE allows nonconformal discretization in the cutting contours. However, half RWG basis functions cannot ensure the continuity of surface current across the cutting contours; therefore, an additional internal penalty term [7, 9] depending on the line integral over

Received 7 June 2019, Accepted 9 August 2019, Scheduled 9 September 2019

* Corresponding author: Qiang-Ming Cai (qmcai@swust.edu.cn).

[1] School of Automation Engineering, University of Electronic Science and Technology of China (UESTC), Chengdu 611731, China. [2] School of Information Engineering, Southwest University of Science and Technology, Mianyang 621010, China. [3] The Department of Electrical and Computer Engineering, Duke University, Durham, NC 27705, USA. [4] EMC Laboratory, Missouri University of Science and Technology, Rolla, MO 65401, USA.

interactions of nonmatching meshes is introduced to enforce this continuity. To improve the capability of modeling complex electrically large objects, the conventional D-formulation VIE (DVIE) [10], E-formulation VIE (EVIE) [11], and VSIE with nonconformal discretization [12, 13] have been developed for dielectric objects and composite objects. In those methods, the local basis functions, e.g., the SWG/RWG basis function [10, 12], the piecewise constant basis [11, 19], have been adopted for expansion and testing. However, the dyadic Green's function in VIE [11] and VSIE [14] can raise hyper-singularity, which needs to be addressed carefully.

In recent years, the J-formulation VIE (JVIE) in terms of equivalent polarization currents J has been proposed for the scattering simulation of anisotropic materials [15], bi-anisotropic materials [16], multilayered materials [17], and highly inhomogeneous materials [18], where the accuracy, flexibility, and efficiency of the JVIE were well demonstrated. It is then preferred over the DVIE and EVIE [15, 19, 20] due to its robustness.

Given the superiority of JVIE and a wider application range in VSIE, to extend this JVIE to VSIE is of great importance for the CMD structures' EM property analysis. Although the SIE and JVIE are respectively introduced in [8, 9] and [18] to support nonconformal discretization, its combination version, i.e., coupling the SIE with J-formulation JVIE, has not been used to construct any form of VSIE with nonconformal discretization yet. To the best of our knowledge, this is the first time that the coupling is applied into the VSIE to simulate CMD structures.

In this paper, we present a novel discontinuous Galerkin (DG) VSIE method (denoted DG-VSIE here), which applies nonconformal meshes conveniently to a complex CMD target through the DG scheme. The reason comes from the nonconformal IE based Galerkin testing process discretized by various types basis functions and supporting various shapes of elements, which is similar to the differential equation with DG method. In fact, the DG methods were first applied to the solution of the differential equation (DE) method, e.g., the finite element method (FEM) [21, 22]. Then, it was extended to the integral equation (IE) to support nonconformal meshes, e.g., IEDG [6] and DGVIE [10]. In this DG-VSIE, the associated equivalent volume currents and surface currents are respectively expanded by CSWG bases and CRWG bases [5], which are defined in curved tetrahedrons and curved triangles. Different from the previous work, our DG-VSIE applies DG-JVIE and DG-SIE respectively to the dielectric part and metallic part, through which the conformal as well as nonconformal meshes can be used for volume and surface discretization. For this proposed DG-VSIE method, several remarks should be given as follows: 1) by introducing half CRWG bases and half CSWG bases in this VSIE, fewer unknowns than the conventional VSIE with CRWG and CSWG bases defined in conformal elements can be obtained; 2) the hyper-singularity problems are avoided by the use of the vector and scaler potentials rather than the dyadic Green's function; 3) a new continuity term [9] is adopted in DG-SIE to enforce the continuity of surface current across the cutting contours, which avoids the introduction of a stabilization term relying on the line integral over interactions of nonmatching meshes; 4) in comparison with the conventional VSIE method, the proposed DG-VSIE shows advantages in alleviating the difficulty of mesh generation and enhancing the accuracy of geometrical modeling. Moreover, fewer unknowns and less simulation time can be obtained by this DG-VISE than that of using nonconformal VSIE with the constant piecewise basis functions [12].

The rest of the paper is organized as follows. Section 2 outlines the basic theories of DG-VSIE. Several numerical results are given in Section 3 to demonstrate its accuracy, efficiency, and flexibility. Section 4 presents a brief conclusion.

2. THEORY

2.1. Volume Surface Integral Equation (VSIE)

As shown in Fig. 1, we assume an arbitrarily shaped three-dimensional CMD structure immersed in a homogeneous background with permittivity ε_b and permeability μ_b. This structure consisting of an inhomogeneous dielectric object V and a metallic surface S is illuminated by an incident field $\mathbf{E}^{inc}(\mathbf{r})$. In the dielectric region V, permeability $\mu(\mathbf{r}) = \mu_b$ and the equivalent complex permittivity $\varepsilon_c(\mathbf{r}) = \varepsilon(\mathbf{r}) - j\sigma(\mathbf{r})/\omega$, where $\varepsilon(\mathbf{r})$ and $\sigma(\mathbf{r})$ denote respectively the permittivity and conductivity.

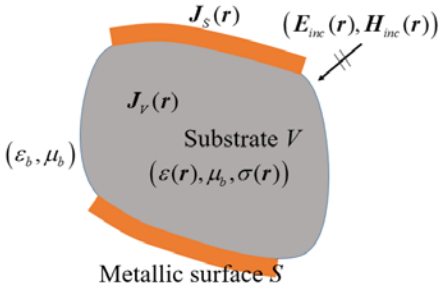

Figure 1. Geometry of a composite structure consisting of an inhomogeneous dielectric object V and a metallic surface S immersed in a homogeneous background medium.

According to the detailed description of [23], the VSIE can be formulated as

$$\mathbf{n} \times [j\omega \mathbf{A}_V(\mathbf{r}) + \nabla \Phi_V(\mathbf{r}) + j\omega \mathbf{A}_S(\mathbf{r}) + \nabla \Phi_S(\mathbf{r}) + \nabla \Phi_C(\mathbf{r})] = \mathbf{n} \times \mathbf{E}^{inc}(\mathbf{r}), \quad \mathbf{r} \in S \tag{1}$$

$$\frac{\mathbf{J}_V(\mathbf{r})}{j\omega \varepsilon_c(\mathbf{r}) \varsigma(\mathbf{r})} + j\omega \mathbf{A}_S(\mathbf{r}) + \nabla \Phi_S(\mathbf{r}) + \nabla \Phi_C(\mathbf{r}) + j\omega \mathbf{A}_V(\mathbf{r}) + \nabla \Phi_V(\mathbf{r}) = \mathbf{E}^{inc}(\mathbf{r}), \quad \mathbf{r} \in V \tag{2}$$

In Eqs. (1) and (2), the vector potentials $\mathbf{A}_S$ and $\mathbf{A}_V$ are respectively defined as

$$\mathbf{A}_S(\mathbf{r}) = \mu_b \int_S \mathbf{J}_S(\mathbf{r}') G(\mathbf{r},\mathbf{r}') dS' \tag{3}$$

$$\mathbf{A}_V(\mathbf{r}) = \mu_b \int_V \mathbf{J}_V(\mathbf{r}') G(\mathbf{r},\mathbf{r}') dV' \tag{4}$$

and the scalar potentials Φ_S, Φ_C and Φ_V are

$$\Phi_S(\mathbf{r}) = -\frac{\eta_b}{jk_b} \int_S \nabla' \cdot \mathbf{J}_S(\mathbf{r}') G(\mathbf{r},\mathbf{r}') dS' \tag{5}$$

$$\Phi_C(\mathbf{r}) = -\frac{\eta_b}{jk_b} \int_C \mathbf{u}_c \cdot \mathbf{J}_S(\mathbf{r}') G(\mathbf{r},\mathbf{r}') dC' \tag{6}$$

$$\Phi_V(\mathbf{r}) = -\frac{\eta_b}{jk_b} \left(\int_V \nabla' \cdot \mathbf{J}_V(\mathbf{r}') G(\mathbf{r},\mathbf{r}') dV' + \int_{S_d^c} \mathbf{n}_c(\mathbf{r}') \cdot (\mathbf{J}_1^V(\mathbf{r}') - \mathbf{J}_2^V(\mathbf{r}')) G(\mathbf{r},\mathbf{r}') \, dS' \right) \tag{7}$$

where $\mathbf{J}_S(\mathbf{r})$ and $\mathbf{J}_V(\mathbf{r})$ represent the equivalent surface current on S and the equivalent volume current in V, respectively. $G(\mathbf{r},\mathbf{r}') = e^{-jk_bR}/4\pi R$ is the Green's function in free space, where $R = |\mathbf{r} - \mathbf{r}'|$ is the distance between the field point $\mathbf{r}$ and source point $\mathbf{r}'$. k_b and η_b denote the wave number and intrinsic impedance of the background, respectively. S_d^c is the interface where the discontinuity of $\varepsilon(\mathbf{r}')$ lies. $\mathbf{n}_c$ is a unit vector normal to S_d^c directed from medium 2 (with current$\mathbf{J}_2(\mathbf{r})$) to medium 1 (with current $\mathbf{J}_1(\mathbf{r})$). $\mathbf{n}$ is the outward unit normal vector on metallic surface S, and $\mathbf{u}_c$ is the in-plane unit normal vectors pointing outwards. $\varsigma(\mathbf{r})$ is the ratio of electric contrast as

$$\varsigma(\mathbf{r}) = \frac{\varepsilon_c(\mathbf{r}) - \varepsilon_b}{\varepsilon_c(\mathbf{r})} \tag{8}$$

Based on the volume equivalent principle [4], the relationship among $\mathbf{J}_V(\mathbf{r})$, the electric filed $\mathbf{E}(\mathbf{r})$ and the electric flux density vector $\mathbf{D}(\mathbf{r})$ is

$$\mathbf{J}_V(\mathbf{r}) = j\omega \varsigma(\mathbf{r}) \varepsilon_c(\mathbf{r}) \mathbf{E}(\mathbf{r}) = j\omega \varsigma(\mathbf{r}) \mathbf{D}(\mathbf{r}) \tag{9}$$

2.2. Geometrical/Current Modeling for DG-VSIE

In this subsection, the geometrical modeling and current modeling will be presented. In the geometrical modeling, the dielectric volume and metallic surface are respectively discretized into the curved

quadratic tetrahedral and triangular elements, whose flexibility makes our VSIE more powerful and attractive. According to [18], a curved quadratic tetrahedral element in physical space (x, y, z) can be described by a second-order transformation from the reference tetrahedron in normalized parent-coordinates $(\xi_1, \xi_2, \xi_3, \xi_4)$. The associated shape function is

$$\begin{aligned}\mathbf{r}(x,y,z) =& 2\xi_1(\xi_1-1)\mathbf{r}_1 + 2\xi_2(\xi_2-1)\mathbf{r}_2 + 2\xi_3(\xi_3-1)\mathbf{r}_3 \quad + 2\xi_4(\xi_4-1)\mathbf{r}_4 + 4\xi_1\xi_2\mathbf{r}_5 + \\ & 4\xi_2\xi_3\mathbf{r}_6 + 4\xi_1\xi_3\mathbf{r}_7 + 4\xi_1\xi_4\mathbf{r}_8 + 4\xi_2\xi_4\mathbf{r}_9 + 4\xi_3\xi_4\mathbf{r}_{10}\end{aligned} \tag{10}$$

where $\mathbf{r_i}$ $(i = 1 \sim 10)$ is the position vector of the quadratic tetrahedral element. Similarly, a curved triangle at the metallic surface can be transformed from the reference triangle in parent-coordinates (ξ_1, ξ_2, ξ_3) [8], with the shape function as

$$\mathbf{r}(x,y,z) = 2\xi_1(\xi_1-1)\mathbf{r}_1 + 2\xi_2(\xi_2-1)\mathbf{r}_2 + 2\xi_3(\xi_3-1)\mathbf{r}_3 + 4\xi_1\xi_2\mathbf{r}_4 + 4\xi_2\xi_3\mathbf{r}_5 + 4\xi_1\xi_3\mathbf{r}_6 \tag{11}$$

where $\mathbf{r_i}$ $(i = 1 \sim 6)$ is the position vector of the quadratic triangular element.

The current modeling process is to discretize the unknown $\mathbf{J}_V(\mathbf{r})$ and $\mathbf{J}_S(\mathbf{r})$ in VSIE by using basis functions. For dielectric part, the JVIE rather than DVIE is discretized. Namely, the unknowns are $\mathbf{J}_V(\mathbf{r})$ rather than $\mathbf{D}(\mathbf{r})$. As suggested by [19, 20], since $\mathbf{J}_V(\mathbf{r})$ do not necessarily satisfy any continuity conditions, basis functions do not enforce any continuity across the element interfaces, which means that some appropriate basis functions belonging to the L^2 (square integral) space can be used to discretize $\mathbf{J}_V(\mathbf{r})$. In JVIE, for a piecewise homogeneous dielectric object, the normal component of $\mathbf{J}_V(\mathbf{r})$ is continuous in the homogeneous part of the object, which can be imposed by CSWG basis functions $\mathbf{f}_n^{VF}(\mathbf{r})$. For the CSWG, if $\xi_1 = 0$, $\mathbf{f}_n^{VF}(\mathbf{r})$ is

$$\mathbf{f}_n^{VF}(\mathbf{r}) = \frac{1}{\Im_V(\xi_1,\xi_2,\xi_3)}\left[\frac{\partial \mathbf{r}}{\partial \xi_1}(\xi_1-1) + \frac{\partial \mathbf{r}}{\partial \xi_2}\xi_2 + \frac{\partial \mathbf{r}}{\partial \xi_3}\xi_3\right] \tag{12}$$

where $\Im_V(\xi_1, \xi_2, \xi_3)$ is the Jacobian factor over a tetrahedron [18]. To model discontinuous currents across the interface between two different media in JVIE, monopolar CSWG basis functions $\mathbf{f}_n^{VH}(\mathbf{r})$ defined over a single tetrahedral element can be utilized, because $\mathbf{J}_V(\mathbf{r})$ has no continuity across material interfaces. Besides, when two neighbouring nonconformal tetrahedrons or their common face does not completely overlap, $\mathbf{f}_n^{VH}(\mathbf{r})$ can be used to represent the $\mathbf{J}_V(\mathbf{r})$ flowing across the cutting contours. With $\mathbf{f}_n^{VF}(\mathbf{r})$ and $\mathbf{f}_n^{VH}(\mathbf{r})$, $\mathbf{J}_V(\mathbf{r})$ can be expanded as

$$\mathbf{J}_V(\mathbf{r}) = \sum_{n=1}^{N_V^F} \alpha_n^v \mathbf{f}_n^{VF}(\mathbf{r}) + \sum_{n=1}^{N_V^H} \beta_n^v \mathbf{f}_n^{VH}(\mathbf{r}) \tag{13}$$

where N_V^F is the number of faces shared by two conformal tetrahedrons, and N_V^H is the number of tetrahedral faces associated with $\mathbf{f}_n^{VH}(\mathbf{r})$. α_n^v and β_n^v are the coefficients of the corresponding basis functions.

On metallic surface S, current $\mathbf{J}_S(\mathbf{r})$ flowing within S can be expanded by CRWG basis functions $\mathbf{f}_n^{SF}(\mathbf{r})$. As $j = 1$, the CRWG $\mathbf{f}_n^{SF}(\mathbf{r})$ can be written as

$$\mathbf{\Lambda}_{00}^1(\mathbf{r}) = \frac{1}{\Im_S(\xi_1,\xi_2)}\left[\frac{\partial \mathbf{r}}{\partial \xi_1}(\xi_1-1) + \frac{\partial \mathbf{r}}{\partial \xi_2}\xi_2\right] \tag{14}$$

where $\Im_S(\xi_1, \xi_2)$ is the Jacobian factor over a triangle [8]. For the current $\mathbf{J}_S(\mathbf{r})$ flowing across the cutting contours can be approximated by monopolar CRWG basis functions $\mathbf{f}_n^{SH}(\mathbf{r})$ defined over a single triangular element. With $\mathbf{f}_n^{SF}(\mathbf{r})$ and $\mathbf{f}_n^{SH}(\mathbf{r})$, $\mathbf{J}_S(\mathbf{r})$ can be expressed as

$$\mathbf{J}_S(\mathbf{r}) = \sum_{n=1}^{N_S^F} \alpha_n^s \mathbf{f}_n^{SF}(\mathbf{r}) + \sum_{n=1}^{N_S^H} \beta_n^s \mathbf{f}_n^{SH}(\mathbf{r}) \tag{15}$$

where N_S^F is the number of edges shared by two conformal triangles, and N_S^H is the number of triangular edges associated with $\mathbf{f}_n^{SH}(\mathbf{r})$. α_n^s and β_n^s are coefficients of the corresponding basis functions.

2.3. DG-VSIE Matrix Equation Based on Nonconformal Discretization

Substituting Eqs. (13) and (15) into Eqs. (1) and (2), and testing with $\mathbf{f}_m^S$ (i.e., $\mathbf{f}_m^{SF}$ and $\mathbf{f}_m^{SH}$) and $\mathbf{f}_m^V$ (i.e., $\mathbf{f}_m^{VF}$ and $\mathbf{f}_m^{VH}$), the matrix equation of VSIE can be obtained as,

$$\begin{bmatrix} \mathbf{Z}^{SS} & \mathbf{Z}^{SV} \\ \mathbf{Z}^{VS} & \mathbf{Z}^{VV} \end{bmatrix} \begin{bmatrix} \mathbf{I}^S \\ \mathbf{I}^V \end{bmatrix} = \begin{bmatrix} \mathbf{V}^S \\ \mathbf{V}^V \end{bmatrix} \tag{16}$$

where $\mathbf{I}^A$ denotes the unknown coefficients, and $\mathbf{V}^A$ is the excitation column-matrix. The sub-matrix $\mathbf{Z}^{AB}$ (A or $B = \{S, V\}$) represents the contribution of the sources in domain B to the field in domain A. With the testing functions $\mathbf{f}_m^S/\mathbf{f}_m^V$ and basis functions $\mathbf{f}_n^S/\mathbf{f}_n^V$, the elements of $\mathbf{V}^A$ can be expressed as

$$V_m^S = \frac{1}{jk_b\eta_b}\int_{S_m} \mathbf{f}_m^S(\mathbf{r})\cdot\mathbf{E}^{inc}(\mathbf{r})dS \tag{17}$$

$$V_m^V = \frac{1}{jk_b\eta_b}\int_{V_m} \mathbf{f}_m^V(\mathbf{r})\cdot\mathbf{E}^{inc}(\mathbf{r})dV \tag{18}$$

The elements of $\mathbf{Z}^{AB}$ are

$$\begin{aligned} Z_{mn}^{SS} = {} & \int_{S_m} \mathbf{f}_m^S(\mathbf{r})\cdot\mathbf{A}_{Sn}(\mathbf{r})\,dS - \frac{1}{k_b^2}\left(\int_{S_m}\nabla\cdot\mathbf{f}_m^S(\mathbf{r})\Phi_{Sn}(\mathbf{r})\,dS + \int_{S_m}\nabla\cdot\mathbf{f}_m^S(\mathbf{r})\Phi_{Cn}(\mathbf{r})\,dS\right. \\ & \left. - \int_{C_m}\left(\mathbf{u}_m\cdot\mathbf{f}_m^{SH}\right)\Phi_{Sn}(\mathbf{r})\,dC - \int_{C_m}\left(\mathbf{u}_m\cdot\mathbf{f}_m^{SH}\right)\Phi_{Cn}(\mathbf{r})\,dC\right) \end{aligned} \tag{19}$$

$$Z_{mn}^{SV} = \int_{S_m} \mathbf{f}_m^S(\mathbf{r})\cdot\mathbf{A}_{Vn}(\mathbf{r})\,dS \tag{20}$$

$$\begin{aligned} Z_{mn}^{VS} = {} & \int_{V_m} \mathbf{f}_m^V(\mathbf{r})\cdot\mathbf{A}_{Sn}(\mathbf{r})\,dV - \frac{1}{k_b^2}\left(\int_{V_m}\nabla\cdot\mathbf{f}_m^V(\mathbf{r})\,\Phi_{Sn}(\mathbf{r})\,dV + \right. \\ & \left. \int_{V_m}\nabla\cdot\mathbf{f}_m^V(\mathbf{r})\Phi_{Cn}(\mathbf{r})\,dV - \int_{S_m}\left(\mathbf{n}_m\cdot\mathbf{f}_m^{VH}\right)\Phi_{Sn}(\mathbf{r})\,dS - \int_{S_m}\left(\mathbf{n}_m\cdot\mathbf{f}_m^{VH}\right)\Phi_{Cn}(\mathbf{r})\,dS\right) \end{aligned} \tag{21}$$

$$\begin{aligned} Z_{mn}^{VV} = {} & -\frac{1}{k_b^2}\int_{V_m}\frac{\mathbf{f}_m^V(\mathbf{r})\cdot\mathbf{f}_n^V(\mathbf{r})}{\varsigma_n(\mathbf{r})\varepsilon_{rn}(\mathbf{r})}dV + \int_{V_m}\mathbf{f}_m^V(\mathbf{r})\cdot\mathbf{A}_{Vn}(\mathbf{r})\,dV \\ & + \frac{1}{k_b^2}\left(\int_{V_m}\nabla\cdot\mathbf{f}_m^V(\mathbf{r})\,\mathbf{\Phi}_{Vn}(\mathbf{r})\,dV - \int_{S_m}\left(\mathbf{n}_m(\mathbf{r})\cdot\mathbf{f}_m^{VH}(\mathbf{r})\right)\,\mathbf{\Phi}_{Vn}(\mathbf{r})\,dS\right) \end{aligned} \tag{22}$$

where $\mathbf{n}_m$ is the outward unit vector normal to S_m of the mth tetrahedral element. $\mathbf{u}_m$ is the in-plane unit normal vectors pointing outwards C_m of the mth triangular element. From Eqs. (3) to (7), potentials $\mathbf{A}_n$ and Φ_n are given by

$$\mathbf{A}_{Sn}(\mathbf{r}) = \int_{S_n}\mathbf{f}_n^S(\mathbf{r}')G\left(\mathbf{r},\mathbf{r}'\right)\,dS' \tag{23}$$

$$\mathbf{A}_{Vn}(\mathbf{r}) = \int_{V_n}\mathbf{f}_n^V(\mathbf{r}')G\left(\mathbf{r},\mathbf{r}'\right)\,dV' \tag{24}$$

$$\Phi_{Sn}(\mathbf{r}) = -\int_{S_n}\nabla'\cdot\mathbf{f}_n^S(\mathbf{r}')G(\mathbf{r},\mathbf{r}')dS' \tag{25}$$

$$\Phi_{Cn}(\mathbf{r}) = -\int_{C_n}\mathbf{u}_n\cdot\mathbf{f}_n^{SH}(\mathbf{r}')G(\mathbf{r},\mathbf{r}')dC' \tag{26}$$

$$\Phi_{Vn}(\mathbf{r}) = -\left(\int_{V_n}\nabla'\cdot\mathbf{f}_n^{VH}(\mathbf{r}')G\left(\mathbf{r},\mathbf{r}'\right)\,dV' + \int_{S_d^c}\mathbf{n}_n(\mathbf{r}')\cdot\mathbf{f}_n^V(\mathbf{r}')G\left(\mathbf{r},\mathbf{r}'\right)\,dS'\right) \tag{27}$$

Note that the divergence theorem $\mathbf{f}_m\cdot\nabla\Phi_n = \nabla\cdot(\Phi_n\,\mathbf{f}_m) - \Phi_n\,\nabla\cdot\mathbf{f}_m$ has been applied in the derivation of $\mathbf{Z}^{AB}$. From Eqs. (23) to (27), it can be found that only weakly singular integrals

are involved and can be easily addressed by existing singularity-handling methods, e.g., the Duffy's transform [24]. Compared to the nonconformal VSIE with constant pricewise basis functions, where the hyper-singularity integrals are contained [11, 12], the above integrals of our DG-VSIE are much easier to calculate. In addition, two remarks are given here. First, the traditional VSIE [23] often requires to generate conformal meshes at the interface of different media, since the continuity condition of the unknown functions should be enforced. However, it is very difficult to generate conformal meshes for high contrast materials or multiscale structures. Our VSIE, fortunately, does not require to enforce the continuity condition at the interfaces between adjacent subdomains for dielectric parts. One reason is that the employed DG-JVIE method [10] has no continuity requirement. $\mathbf{f}_n^{VH}(\mathbf{r})$ is used for single elements lied on the interfaces between nonconformal or different media domains. The other reason is that $\mathbf{f}_n^{VH}(\mathbf{r})$ is defined over the volume, rather than on the surface, and the application of $\mathbf{f}_n^{VH}(\mathbf{r})$ to both nonconformal and different media domains will only generate surface charge densities, instead of the line charge densities. This suggests that no singular field will be produced by applying $\mathbf{f}_n^{VH}(\mathbf{r})$ to above two sceneries. Metallic surface is discretized by $\mathbf{f}_n^{SH}(\mathbf{r})$, as defined over single triangular elements near the cutting contours. Because $\mathbf{f}_n^{SH}(\mathbf{r})$ cannot ensure the continuity of $\mathbf{J}_S(\mathbf{r})$ across the cutting contours, an additional continuity term [9] is introduced to enforce this continuity in this DG-VSIE. The electric potential generated by error electric charges can be expressed as

$$\Phi_{err}(\mathbf{r}) = -\frac{j\omega}{k_b^2}\sum_{n=1}^{N}\int_{C_n}\mathbf{u}_n\cdot\mathbf{f}_n^{SH}(\mathbf{r}')G(\mathbf{r},\mathbf{r}')dC' \tag{28}$$

Then, surface electric charges $\nabla\cdot\mathbf{J}_S(\mathbf{r}) = -j\omega\rho_s$ or line electric charges $\mathbf{u}\cdot\mathbf{J}_S(\mathbf{r}) = -j\omega\rho_l$ on metallic surface S are adopted to test the error electric potential $\Phi_{err}(\mathbf{r})$ and make them equal to zero, i.e.,

$$\frac{1}{k_b^2}\int_{C_m}\left(u_m\cdot f_m^{SH}\right)\Phi_{err}(r)\,dC = 0 \tag{29}$$

$$\frac{1}{k_b^2}\int_{S_m}\nabla\cdot f_m^{S}\,\Phi_{err}(r)\,dS = 0 \tag{30}$$

Physically, Eqs. (29) and (30) mean that the electric potential energy generated by the accumulated error charges at the cutting contours vanishes. Thus, a continuity term has been used in the DG-VSIE system to minimize the electric potential energy associate with the error charges accumulated at the cutting contours. On the other hand, it should be pointed out that the use of half basis functions and full basis functions for nonconformal and conformal domains will reduce unknowns to compute.

3. NUMERICAL RESULTS

In this section, numerical examples are given to validate the accuracy and efficiency of the DG-VSIE. All the simulations are performed on a personal computer with 4.0-GHz Intel(R) Core(TM) I7-4790K CPU. The conjugate gradient method (CGM) with an iterative tolerance 0.001 is used to solve the VSIE equation.

3.1. Metallic Sphere with Coatings

To investigate the accuracy of this DG-VSIE method, the first example is to simulate the EM scattering from a metallic sphere with a two-layer dielectric coating as shown in Fig. 2(b), where the relative permittivities for the two coatings are respectively $\varepsilon_{r1} = 2.0$ and $\varepsilon_{r2} = 4.0$. The radius of the metallic core sphere is 0.3 m, and the thicknesses of the first and second layers are respectively 0.03 m and 0.02 m. The nonconformal meshing yields 7152 tetrahedrons and 1020 triangles, where the average mesh sizes for the dielectric layers 1 and 2 are respectively $\lambda_0/(10\sqrt{\varepsilon_{r1}})$ and $\lambda_0/(10\sqrt{\varepsilon_{r2}})$, and for the metallic surface elements is $\lambda_0/10$. The nonconformal meshes for this structure are shown in Fig. 2(a). This structure is illuminated by a plane wave at frequency 300 MHz. By using CSWG/CRWG bases, the DG-VSIE results in 18184 unknowns and takes 3338 s. For comparison, the conventional VSIE employs SWG/RWG bases in conformal planar discretization and produces 20,165 unknowns under the same

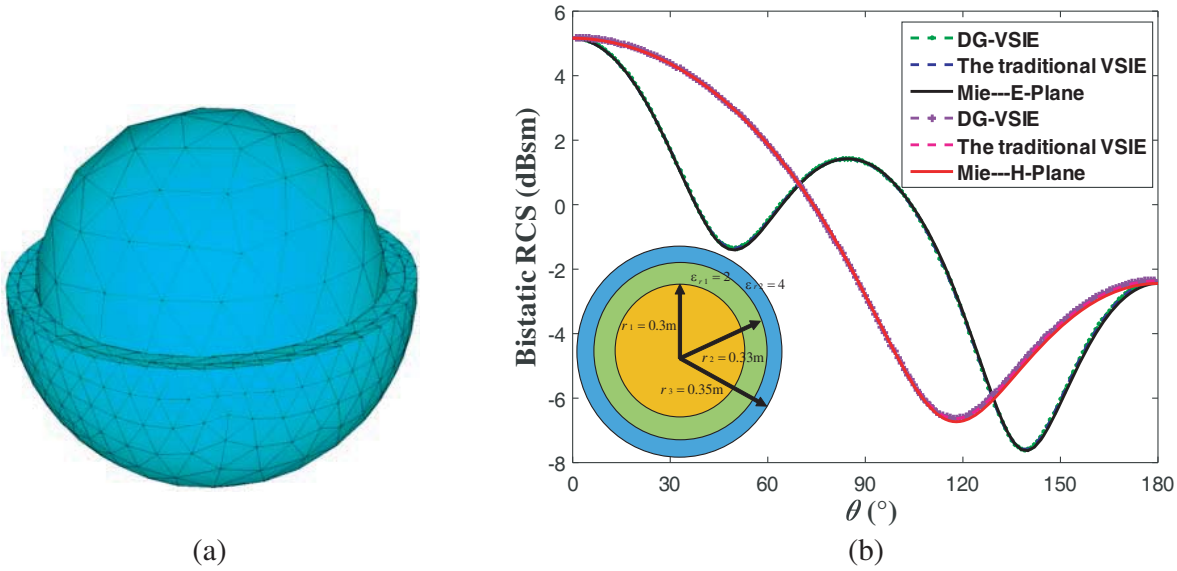

Figure 2. Nonconformal modelling of a metallic sphere with two-layer coatings. (a) Cross-section of the nonconformal mesh along the center plane. (b) Comparison of the bistatic RCS (E- and H-plane) among the DG-VSIE, the traditional VSIE and the Mie series.

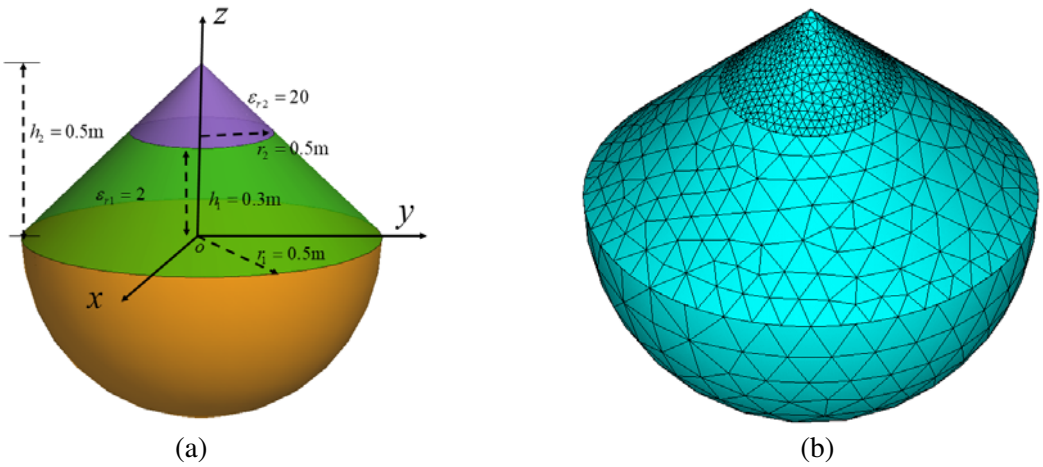

Figure 3. (a) Geometry and (b) nonconformal discretization with curved geometrical modeling for the composite cone-sphere target.

mesh sizes. As shown in Fig. 3, the bistatic RCS of the DG-VSIE coincides with those of the conventional VSIE as well as the Mie series. To further measure the accuracy of this VSIE, the root mean square (RMS) error [5, 25] of the bistatic RCS is defined here, i.e.,

$$\text{RMS error (dB)} = \sqrt{\frac{1}{N_a}\sum_{i=1}^{N_a}\left|\sigma_{cal,i} - \sigma_{ref,i}\right|^2} \tag{31}$$

where $\sigma_{cal,i}$ denotes the Bistatic RCS calculated by the proposed VSIE, and $\sigma_{ref,i}$ is the reference results obtained from either Mie's series or commercial software FEKO 2017 [26]. The results calculated by FEKO are based on the traditional conformal MoM-VSIE with RWG/SWG basis functions. N_a represents the number of sampling points. Both $\sigma_{cal,i}$ and $\sigma_{ref,i}$ are in decibels. To illustrate the results' difference between our VSIE and the traditional VSIE, the average mesh sizes are respectively set to $\lambda_0/(10\sqrt{\varepsilon_r})$ and $\lambda_0/10$ for the dielectric volume and metallic surface elements. In addition,

the definition of RMS error in Eq. (31) shows that the error monotonously varies with $(\hat{\sigma}_{cal,i}/\hat{\sigma}_{ref,i})$, where $\sigma_{cal,i} = 10\log\hat{\sigma}_{cal,i}$ and $\sigma_{ref,i} = 10\log\hat{\sigma}_{ref,i}$, implying that an increasing RMS error means a larger difference between $\hat{\sigma}_{cal,i}$ and $\hat{\sigma}_{ref,i}$. Thus, the RMS error of Eq. (31) can be used to measure the accuracy of solutions. The RMS errors for the E- and H-plane cases for our VSIE are respectively 0.13 dB and 0.15 dB, while those for the conformal VSIE are respectively 0.12 dB and 0.18 dB. The number of unknowns in the DG-VSIE is less than that in the conventional VSIE, while the accuracy keeps the same level. Besides, note again that the proposed VSIE is discretized by CRWG/CSWG bases, which are defined on curved triangular/tetrahedral elements. Although curved elements can enhance the accuracy of geometrical modelling, the singularity integral process over the curved elements becomes more challenging, than that of the planar elements [5]. In this example, the Duffy's transform [24] is adopted to address the existing singularity integrals. The singularity subtraction technique [27] is used in the traditional conformal VISE to handle the singular and near-singular integrals to guarantee the solution precision. Note that the near-singular integrals are not handled in this paper, which may decrease the integral accuracy, as observed from the RMS error of the E-plane.

3.2. Composite Cone-Sphere Target

In the second example, a composite object with sharp features, including a dielectric cone of 0.5-m height and a metallic hemisphere of 0.5 m radius, is illuminated by a plane wave $\mathbf{E}^{inc}(\mathbf{r}) = \mathbf{e}_x e^{-jk_b z}$ at 300 MHz. As shown in Fig. 3(a), the dielectric cone has two parts (the relative permittivity $\varepsilon_{r1} = 2.0$ and $\varepsilon_{r2} = 20.0$) and is meshed independently by curved tetrahedral elements with different edge lengths, i.e., $\lambda_0/(10\sqrt{\varepsilon_{r1}})$ and $\lambda_0/(10\sqrt{\varepsilon_{r2}})$ (λ_0 is the wavelength in free space); the hemisphere is meshed by curved triangular elements with the average mesh size $\lambda_0/10$. The nonconformal discretization shown in Fig. 3(b) produces 9,906 volumetric elements and 742 surface elements. In use of DG-VISE with CSWG/CRWG bases, the total unknowns and memory usage are respectively 22,210 and 3,428 MB, and the CPU time is 3,077 s. Fig. 4 shows good agreement between the bistatic RCS results from the DG-VSIE with the nonconformal discretization and the traditional VSIE (38,309 unknowns and 4,112 MB memory usage) with the conformal mesh grids in the same mesh size, which verifies the correctness of this approach for structures with sharp features. Benefitting from the NBF technique [18], our VSIE only requires 534 iterations to reach a relative residual of 0.001; otherwise, 813 iterations are required. Moreover, the scattering of the composite target without the small dielectric cone part, whose relative permittivity $\varepsilon_{r2} = 20.0$, is also computed, as shown in Fig. 4. It can be found that the fine structure involving high-contrast media indeed has important influence on the far-field results. This

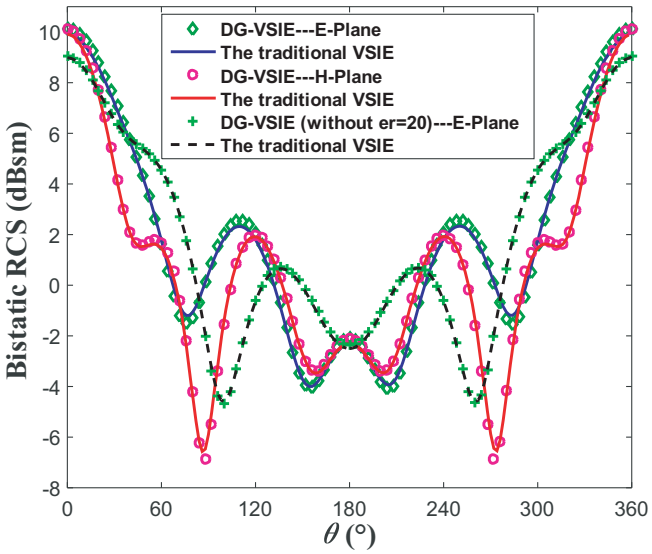

Figure 4. Comparison of the bistatic RCS (E- and H-plane) for a cone-sphere composite object between the DG-VSIE and the traditional VSIE.

also demonstrates that the proposed VSIE can successfully capture the influence. Besides, note again here that the use of nonconformal meshes makes the DG-VSIE a much more flexible and efficient solver than the traditional VSIE method, especially for inhomogeneous high permittivity contrast dielectric objects.

3.3. Microstrip Patch Antenna

A patch antenna [5] is modeled as the third example in Fig. 5 and illuminated by a plane wave $\mathbf{E}^{inc}(\mathbf{r}) = \mathbf{e}_x e^{-jk_b z}$ at 3.0 GHz. The dielectric substrate and metallic patch of the antenna are independently meshed with an average mesh size $\lambda_D/10$ (λ_D is the dielectric wavelength) and $\lambda_0/10$, generating 916 triangles and 2,918 tetrahedrons in total. The DG-VSIE then employs 8,328 unknowns, 536 MB memory, and 603 s CPU time to compute the bistatic RCS and agrees with the results from commercial software FEKO in Fig. 6(a). The FEKO employs the conformal VSIE based on SWG/RWG bases and yields 9,374 unknowns, 678 MB memory usage, and 912 s CPU time.

Therefore, we can conclude that the DG-VSIE method outperforms the traditional VSIE with a lighter computational burden. Besides, with the help of NBF technique [18], faster convergence speed can be achieved by our VSIE to reach the iterative tolerance 0.001, compared with that of the conformal VSIE of 1513 iteration steps. Besides, it should be noted that the direct solvers, e.g., LU solver or Gaussian solver, are often used in conventional VSIE, mainly because slow convergence is observed when iterative solvers are utilized to simulate multiscale and ill-conditioned CMD structures, e.g., the microstrip antenna [23].

In order to further illustrate the accuracy and the ability of our DG-VSIE, the far-fields radiation of the patch antenna excited by a probe with a 50 Ohm port is calculated. In the radiation process, the simulation parameters, e.g., the working frequency, and the nonconformal mesh size are the same as the above scattering process. Besides, the probe is represented by a small cube with the height 0.2362 cm, the width and length 0.3 cm. A 1-V source is placed across a delta gap in each fed-edge. Fig. 6(b) compares the normalized far-field radiation results calculated by the DG-VSIE with the reference results from FEKO based on the traditional VSIE. Good agreement between them is observed. Based on the above discussions, to summarize, this example demonstrates the accuracy and verification of the proposed DG-VSIE for the scattering and radiation simulation of CMD structures.

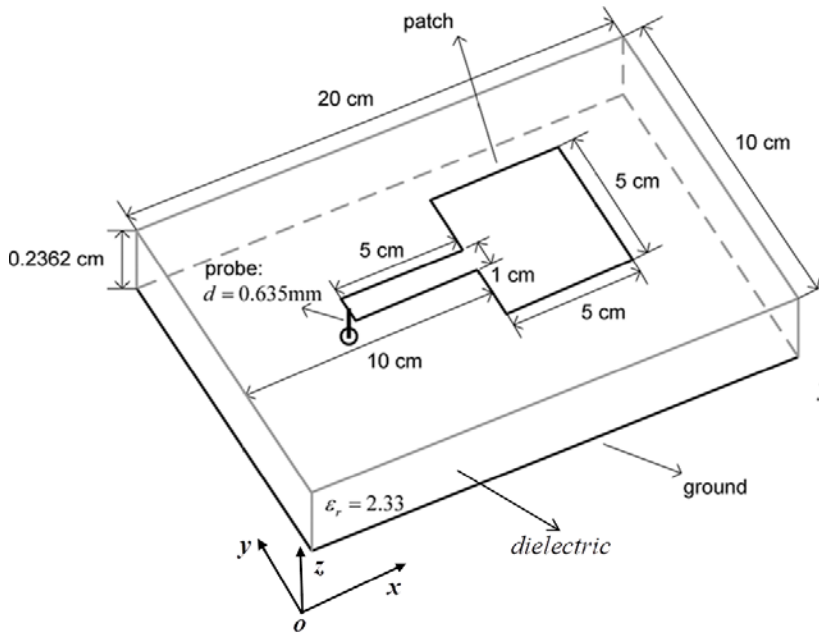

Figure 5. Geometry and dimensions of the patch antenna simulated in [5].

3.4. Monopole Antenna with Hemispherical Radome

The last example is a multiscale structure, including a monopole antenna placed on a metallic circle and a two-layers hemispherical radome as shown in Fig. 7(a). For the radome, the thicknesses and relative permittivities of the first and second inner layers are respectively $\tau_1 = 5.0\,\text{mm}$ and $\varepsilon_{r1} = 2 - 0.005j$, and $\tau_2 = 5.0\,\text{mm}$ and $\varepsilon_{r2} = 1.5 - 0.035j$. The diameter D of the radome is 500 mm. The monopole antenna of 1.0-mm radius is located at the center of a metallic circle disk, whose diameter is 800 mm. In this simulation, this monopole antenna is represented by a small cube of the height 125.0 mm, the width and length 4.0 mm. The average mesh sizes for the radome, monopole antenna, and circle disk are $\lambda_0/(10\sqrt{\varepsilon_{ri}})$ $(i = 1, 2)$, $0.005\lambda_0$, and $0.1\lambda_0$, respectively. As shown in Figs. 7(b) and (c), the nonconformal discretization is used, which generates 4582 tetrahedrons and 560 triangles. The excitation is a 3.0 GHz x-polarized plane wave incident along $-z$-axis. With the use of DG-VISE, the resulting unknown number and memory consumption are respectively 11,646 and 1,043 MB, and the required computational cost is 1,203 s with 904 iteration steps. As plotted in Fig. 8, bistatic RCS obtained by the DG-VSIE agrees well with the results of FEKO. Thus, the high accuracy of the VSIE is demonstrated. It is also evident that the DG-VSIE is superior in the scattering simulation of multiscale antennas.

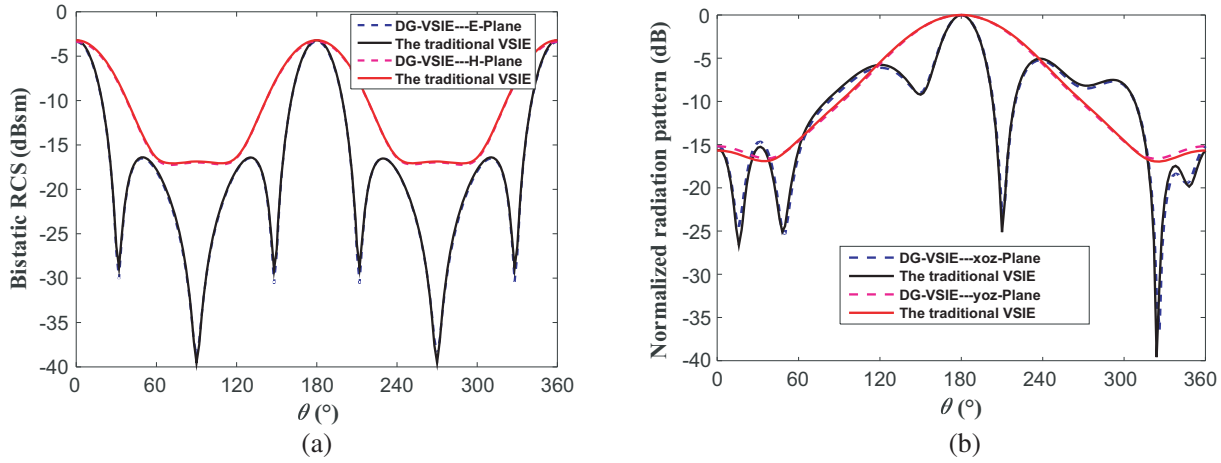

Figure 6. Nonconformal modelling of a patch antenna. (a) Comparison of the bistatic RCS (E- and H-plane) obtained by the proposed DG-VSIE and FEKO based the traditional VSIE. (b) Comparison of the normalized radiation patterns (xoz- and yoz-plane) calculated by the DG-VSIE and the software FEKO with the traditional VSIE.

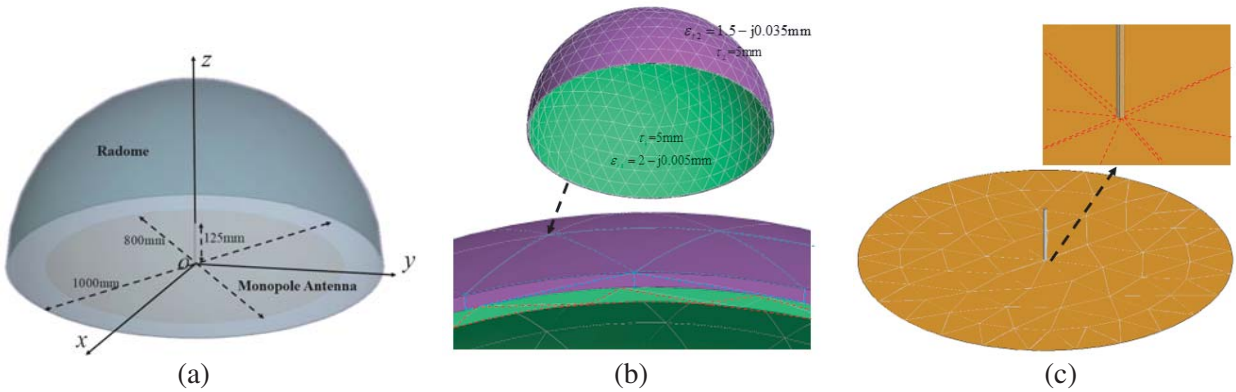

Figure 7. (a) The structure of a monopole antenna with hemispherical radome. (b) Nonconformal discretization with curved geometrical modeling for radome. (c) Nonconformal discretization with curved geometrical modeling for monopole antenna.

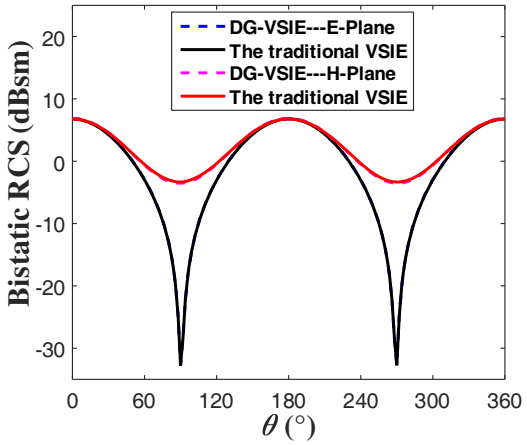

Figure 8. Comparison of bistatic RCS of the monopole antenna with hemispherical radome in the *xoz*- and *yoz*-plane. The results from DG-VSIE are compared with the reference results simulated by the commercial software FEKO based on the conventional VSIE.

4. CONCLUSION

A novel DG-VSIE scheme based nonconformal discretization is presented to simulate the EM scattering from CMD structures. By using curved tetrahedral elements and curved triangular patches for geometric modeling and the associated CRWG (CSWG) basis functions for surface (volume) current modeling, the DG-VIE method and DG-SIE approach are adopted for dielectric volume and metallic surface, respectively. Thus, the conformal as well as non-conformal volume/surface discretization can be allowed in this VSIE. Obviously, the non-conformal nature of the VSIE gives the considerable flexibility in the meshing.

The DG-VSIE has been utilized to solve the EM scattering of a metallic sphere coated with high contrast dielectric materials, a patch antenna, and a monopole antenna with hemispherical radome. The associated simulation results agree well with the Mie series and/or the results obtained by the conventional VSIE, while our DG-VSIE method requires less computational cost for the same accuracy level than the conventional VSIE. In summary, the DG-VSIE can serve as an accurate, efficient, and flexible alternative to the commonly used VSIE for the EM simulation of CMD structures, especially when involving multiscale structures or high contrast dielectric media.

ACKNOWLEDGMENT

This work is supported in part by the National Natural Science Foundation of China (No. 61801406).

REFERENCES

1. Ouyang, J., F. Yang, S. W. Yang, and Z. P. Nie, "Exact simulation method VSWIE-MLFMA for analysis radiation pattern of probe-feed conformal microstrip antennas and the application of synthesis radiation pattern," *Journal of Electromagnetic Waves and Application*, Vol. 21, No. 14, 1995–2008, 2007.
2. Yuan, N., T. S. Yeo, X. C. Nie, Y. B. Gan, and L. W. Li, "Analysis of probe-fed conformal microstrip antennas on finite grounded substrate," *IEEE Trans. Antennas Propag.*, Vol. 54, No. 2, 554–563, Feb. 2006.
3. Rao, S. M., D. R. Wilton, and A. W. Glisson, "Electromagnetic scattering by surfaces of arbitrary shape," *IEEE Trans. Antennas Propag.*, Vol. 30, 409–418, May 1982.

4. Schaubert, D. H., D. R. Wilton, and A. W. Glisson, "A tetrahedral modeling method for electromagnetic scattering by arbitrarily shaped inhomogeneous dielectric bodies," *IEEE Trans. Antennas Propag.*, Vol. 32, 77–85, Jan. 1984.
5. Cai, Q.-M., Y.-W. Zhao, W.-F. Huang, Y.-T. Zheng, Z.-P. Zhang, Z.-P. Nie, and Q. H. Liu, "Volume surface integral equation method based on higher order hierarchical vector basis functions for EM scattering and radiation from composite metallic and dielectric structures" *IEEE Trans. Antennas Propag.*, Vol. 64, No. 12, 5359–5372, Dec. 2016.
6. Peng, Z., K.-H. Lim, and J.-F. Lee, "A discontinuous Galerkin surface integral equation method for electromagnetic wave scattering from nonpenetrable targets," *IEEE Trans. Antennas Propag.*, Vol. 61, No. 7, 3617–3628, Jul. 2013.
7. Wang, X. C., Z. Peng, and J. F. Lee, "A new integral equation based domain decomposition method for electromagnetic analysis of large multi-scale problems," *Proc. IEEE Antennas Propag. Soc. Int. Symp. (APSURSI'12)*, 1–2, Jul. 2012.
8. Cai, Q.-M., Y.-W. Zhao, L. Gu, Z. -P. Nie, and Q. H. Liu, "Analysis of multi-scale problems from PEC objects by a discontinuous Galerkin SIE based on higher order hierarchical vector basis functions," *Proc. Int. IEEE AP-S Symp.*, 1611–1612, 2016.
9. Han, K., Y. Chen, X. Que, et al., "A domain decomposition scheme with curvilinear discretizations for solving Large and complex PEC scattering problems," *IEEE Antennas Wireless Propag. Lett.*, Vol. 17, 242–246, 2018.
10. Zhang, L. M. and X. Q. Sheng, "Discontinuous Galerkin volume integral equation solution of scattering from inhomogeneous dielectric objects by using the SWG basis function," *IEEE Trans. Antennas Propag.*, Vol. 65, 1500–1504, Mar. 2017.
11. Ozdemir, N. A. and J.-F. Lee, "A nonconformal volume integral equation for electromagnetic scattering from penetrable objects," *IEEE Trans. Magn.*, Vol. 43, No. 4, 1369–1372, Apr. 2007.
12. Ng, T.-H., J.-F. Lee, Z. Peng, and K. H. Lim, "A non-conformal volume surface integral equation for electromagnetic scatterings from composite PEC and inhomogenous anisotropic scatterers," *Proc. IEEE APS Int. Symp. Dig.*, 728–729, Oct. 2013.
13. Li, X. J., L. Lei, et al., "VSIE-based domain decomposition method with simplified prism vector basis functions for planar thin dielectric-conductor composite objects," *IEEE Antennas Wireless Propag. Lett.*, Vol. 17, 1608–1612, Sep. 2018.
14. Tong, M. S., Z. G. Qian, and W. C. Chew, "Nyström method solution of volume integral equations for electromagnetic scattering by 3D penetrable objects," *IEEE Trans. Antennas Propag.*, Vol. 58, No. 5, 1645–1652, May 2010.
15. Markkanen, J., P. Ylä-oijala, and A. Sihvola, "Discretization of volume integral equation formulations for extremely anisotropic materials," *IEEE Trans. Antennas Propag.*, Vol. 60, No. 11, 5195–5202, Nov. 2012.
16. Ylä-Oijala, P., J. Markkanen, and S. Järvenpää, "Current-based volume integral equation formulation for bianisotropic materials," *IEEE Trans. Antennas Propag.*, Vol. 64, No. 8, 3470–3477, Aug. 2016.
17. Schols, Y. and G. A. E. Vandenbosch, "Separation of horizontal and vertical dependencies in a surface/volume integral equation approach to model quasi 3-D structures in multilayered media," *IEEE Trans. Antennas Propag.*, Vol. 55, No. 4, 1086–1094, Apr. 2007.
18. Cai, Q.-M., Z.-P. Zhang, Y.-W. Zhao, W.-F. Huang, Y.-T. Zheng, Z.-P. Nie, and Q. H. Liu, "Nonconformal discretization of electric current volume integral equation with higher order hierarchical vector basis functions," *IEEE Trans. Antennas Propag.*, Vol. 65, No. 8, 4155–4169, Aug. 2017.
19. Markkanen, J. and P. Ylä-Oijala, "Discretization of electric current volume integral equation with piecewise linear basis functions," *IEEE Trans. Antennas Propag.*, Vol. 62, No. 9, 4877–4880, Sep. 2013.
20. van Beurden, M. C. and S. J. L. van Eijndhoven, "Well-posedness of domain integral equations for a dielectric object in homogeneous background," *J. Eng. Math*, Vol. 62, 289–302, 2008.

21. Houston, P., I. Perugia, and D. Schötzau, "An a posteriori error indicator for discontinuous Galerkin discretizations of (curl)-elliptic partial differential equations," *IMA J. Numer. Anal.*, Vol. 27, No. 1, 122–150, 2007.
22. Arnold, D., "An interior penalty finite element method with discontinuous elements," *SIAMJ. Numer. Anal.*, Vol. 19, No. 4, 742–760, 1982.
23. Lu, C. C. and W. C. Chew, "A coupled surface-volume integral equation approach for the calculation of electromagnetic scattering from composite metallic and material targets," *IEEE Trans. Antennas Propag.*, Vol. 48, No. 12, 1866–1868, Dec. 2000.
24. Duffy, M. G., "Quadrature over a pyramid or cube of integrands with a singularity," *SIAM J. Numer. Anal.*, Vol. 19, No. 6, 1260–1262, Dec. 1982.
25. Gang, K., J. M. Song, W. C. Weng, K. C. Donepudi, and J. M. Jin, "A novel grid-robust higher order vector basis function for the method of moments," *IEEE Trans. Antennas Propag.*, Vol. 49, No. 6, 908–915, Jun. 2001.
26. Altair Feko, Altair Engineering, Inc., www.altairhyperworks.com/feko.
27. Järvenpää, S., M. Taskinen, and P. Ylä-Oijala, "Singularity subtraction technique for high-order polynomial vector basis functions on planar triangles," *IEEE Trans. Antennas Propag.*, Vol. 54, No. 1, 42–49, Jan. 2006.